Global and local endmembers spectral patterns to estimate the urban structure in Porto Alegre (Brazil) in Landsat images using the Linear Spectral Mixture Model procedure

Mayumi Cursino de Moura Hirye [1], Eliana Lima da Fonseca [2]

[1] Institute of Environment and Sustainability, University of California, Los Angeles – CA, United States – mhirye@ucla.edu
[2] Laboratório de Geotecnologias Aplicadas, Department of Geography, Federal University of Rio Grande do Sul, Porto Alegre – RS, Brazil – eliana.fonseca@ufrgs.br

Keywords: Urban remote sensing, Urban vegetation, Unmixed model, Sub-pixel, Google Earth Engine

Abstract

This study investigates the spectral patterns of global and local endmembers to assess urban structure estimation within Porto Alegre city, Brazil. Two distinct sets of endmembers were examined: one derived from global patterns acquired from 100 Landsat image subsets and the other from local patterns gathered across 27 analyzed images. Results reveal that the utilization of global endmember patterns tends to overestimate the presence of urban shadow in all analyzed images compared to estimates derived from local patterns. Consequently, this overestimation impacts the relative proportions of other endmembers. Despite the disparities in magnitude between fractions estimated with each set of endmembers, temporal variations exhibit similar interannual trends. The findings of this study suggest that, beyond the choice between standardized or localized models, the features that must be represented in the resulting maps should also be considered in the selection between global and local endmembers.

1. Introduction

Porto Alegre city (30°1'S, 51°13'W) has 495 km^2 with around 1.3 million inhabitants, resulting in a population density of around 2600 inhab/km^2 according to the last Brazilian census, carried out in 2023 (IBGE, 2024). Porto Alegre is the capital city of Rio Grande do Sul, Brazil's southernmost state (Figure 1). Like many other big cities worldwide, Porto Alegre faces environmental and social challenges, such as heat island effect, air pollution and social inequality. This social inequality exacerbates the low incoming families' vulnerability to climate change impacts (Gonçalves et al., 2020). Porto Alegre's climate is Cfa, according to the Köppen classification, without a dry season and with hot summers. The city is often hit by heat waves during summer (Stefanello et al., 2022), with temperatures close to 40oC and higher thermal sensation. Hence, monitoring urban afforestation is crucial for enhancing urban resilience to climate change by leveraging the benefits of vegetation presence and reducing vulnerability to climate stress. It also can play a role in advancing environmental justice by supporting a better distribution of green spaces within urban areas.

The afforestation in the Porto Alegre city streets’ began in the first half of the 20th century. According to the Brazilian census carried out in 2010, there are trees in front of 82.7% of urban houses in this city (IBGE, 2024). Nevertheless, according to environmental activists, ten trees have been cut down every day in this city in recent years. One of the reasons for these cuts is that older trees have a large structure of stems and branches (Boeni and Silveira, 2019), which increases the risk of those trees falling on buildings and vehicles during the intense storms that occur in this region every year. On the other hand, urban trees play an essential role in controlling temperature within urban areas, also affecting ambient temperature and the human response to heat stress (Salbitano et al., 2016). Pervious areas covered with vegetation maintain soil infiltration capacity, decreasing the impact of the urban growth on the runoff and contributing to effective stormwater management by mitigating flooding and preserving the natural hydrological cycle (Campana & Tucci, 2001).

The use of satellite images for monitoring intra-urban vegetation in a systematic way is limited by the spatial resolution of the images. Some aspects can be monitored with moderate-resolution images, like the phenological cycle of vegetation, controlled by meteorological variables, that can be monitored inside the urban areas using the MODIS sensor, with 250 meters of spatial resolution in the red and near-infrared bands (Zhang et al., 2003; Zhang et al., 2022). With a spatial resolution of 30 meters and a temporal resolution of 16 days, Landsat satellite images are possible to identify the tree canopies (Wang, 1988; Nölke, 2021) with some limitations regarding the spatial resolution. In some cases, the Landsat images were fused with higher resolution images like Planet Scope, (Twumasiet al., 2022) to improve the ability to detect isolated trees in urban areas. Very high-resolution imagery can be used to identify tree height (Tola et al., 2023) and even trees species within urban environments (Pinheiro et al., 2020), enabling detailed analysis and improved management of urban vegetation.

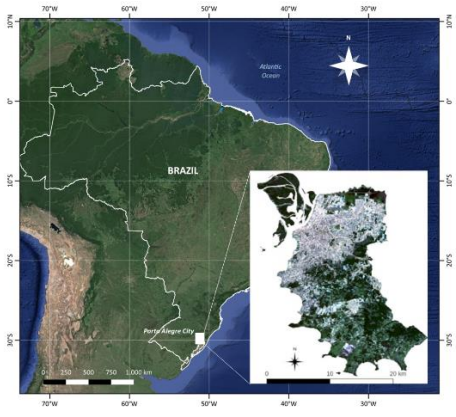

Figure 1 – Location map

Image processing techniques, like the Linear Spectral Mixture Model (LSMM), also known as Linear Spectral Mixture Analysis (LSMA), can retrieve information at a sub-pixel level. The LSMM (Equation 1) considers that the response of each resolution unit of the image (pixel) in any spectral band is the linear combination of the responses of the targets (endmembers) that occurs inside the resolution unit on the ground (Shimabukuro and Smith, 1991).

$$r_i = \sum_{j=1}^{n} (a_{ij} x_j) + e_i \qquad (1)$$

Where r = pixel spectral reflectance
a = endmember spectral reflectance
x = proportion value of the endmember in the pixel
e = error term
j = number of endmembers
i = number of spectral bands

The LSMM output is one image for each endmember, called “fraction-images” or “abundance-images”. In an abundance image, each pixel presents the proportion of each endmember (x_j) in the interior of this pixel. Also, the sum of the proportions for each pixel considering all the abundance-images is 100%. A LSMM analysis requires *a priori* knowledge of the spectral patterns of targets present in the area of interest (Heinz and Chang, 2001). Endmembers’ spectral patterns can be collected directly from the analyzed images, and this approach presents some advantages, such as being easy to obtain and being at the same scale as the image data (Quintano et al., 2012).

The LSMM procedure can be used in the Landsat images in urban areas to estimate the urban vegetation abundance (Small, 2001), and to improve the classification results, using the abundance-images with the other information derived from the images to map the urban trees (Lu and Weng, 2004; Lu and Weng, 2005). This procedure can also identify the land use urban classes, which differ from land cover classes usually used in regional maps (Guindon et al., 2004).

This work aims to analyze global and local endmembers spectral patterns datasets, both collected directly from Landsat images, to estimate the built-up structures inside the urban areas in Porto Alegre city (Brazil) based on the LSMM analysis and Landsat imagery. These analyses allow a better understanding of how useful the global endmembers' spectral patterns are in applying the LSMM in different Brazilian cities in an operational way when compared with local endmembers' spectral patterns collected over each analyzed city.

2. Methodology

The analysis was made using Google Earth Engine (GEE) with its native Javascript interface (Gorelick et al., 2017) and Landsat-8 (OLI sensor) imagery. All the methodological steps in the workflow are presented in Figure 2. A time-series imagery was generated with all cloud-free Landsat 8 images (*USGS Landsat 8 Level 2, Collection 2, Tier 1),* acquired over Porto Alegre from 2014 to 2021 (*path*/*row* 221/81). The selection was made based on the metadata selection (“*cloud cover*” less than 0%) and visual inspection, resulting in a 27-image time ‘’series. The OLI sensor has six optical bands, with 30 meters spatial resolution (Band 2 – Blue, Band 3 – Green, Band 4 – Red, Band 5 – Near infrared, Band 6 – Shortwave infrared, Band 7 – Shortwave infrared) which were used as input data for the LSMM.

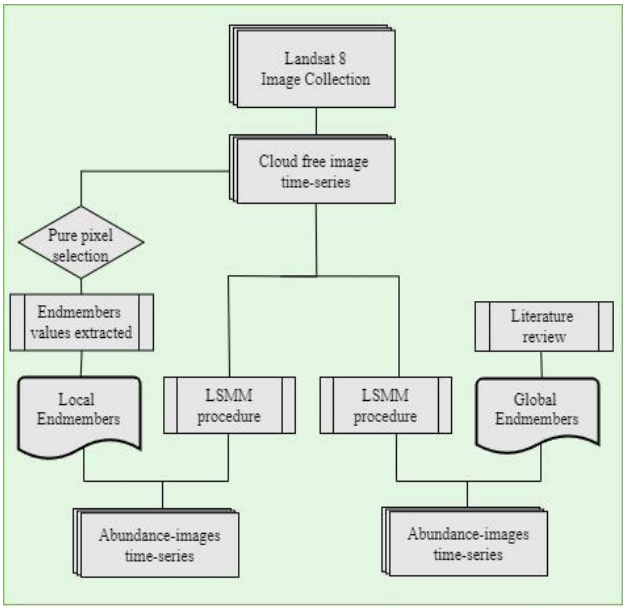

Figure 2. Methodology workflow

Two different sets of endmembers spectral patterns were tested to perform the LSMM. One dataset is composed of global spectral patterns acquired over 100 Landsat image subsets (Small and Milesi, 2013) and the other dataset is composed of local patterns collected over Porto Alegre, using the analyzed time-series images. Both datasets were generated by collecting spectral patterns based on the pure pixel concept, i.e., a pixel with only one target inside. The global patterns (Table 1) were generated by collecting spectral information over 100 subsets with different targets inside and the principal components procedure was used to identify the endmembers spectral patterns for vegetation, substrate and dark targets (Small and Milesi, 2013).

Three points were selected over the following longitudes and latitudes: (-51.228014, -30.029546) for urban shade; (-51.219815, -30.069096) for urban vegetation; and (-51.203262, -30.060039) for urban built-up structures to collect the local endmembers spectral patterns. These points were the same for all the time-series and were selected based on the visual inspection and user experience. The spectral patterns were collected for each image, and the median value of the 27 images analyzed for each endmember was used to perform the LSMM analysis (Table 1).

The LSMM was performed to estimate the proportion of three endmembers, namely urban vegetation, urban shade and urban built-up structures over Porto Alegre city. The output was three images, called “abundance-images,” showing the proportion of each endmember within each pixel. The LSMM is implemented in GEE (unmixed command) and was used with the following restrictions: A) the sum of the fraction images generated must be equal to one in the same pixel; B) no fraction can be negative (Shimabukuro and Smith, 1991). The two endmembers’ datasets were used, generating two abundance-images datasets for each of the 27 dates analyzed, from 2014 to 2021, which were analyzed and compared.

Endmembers	Landsat bands					
	B2	B3	B4	B5	B6	B7
Global						
Substrate	0.178	0.337	0.458	0.559	0.683	0.645
Dark	0.019	0.010	0.005	0.007	0.003	0.002
Vegetation	0.030	0.060	0.031	0.669	0.240	0.096
Local						
Urban built-up	0.060	0.085	0.117	0.193	0.280	0.235
Urban shadow	0.023	0.030	0.030	0.041	0.061	0.059
Urban vegetation	0.018	0.035	0.023	0.302	0.100	0.038

Table 1. Global and local endmembers reflectance spectral patterns values for the Landsat 8 optical bands.

3. Results and discussion

The endmembers spectral patterns (Table 1) show different values for each dataset (global and local) across all Landsat bands. To better analyze the spectral patterns a graph considering the central wavelength for each Landsat band is presented in Figure 3. Both vegetation patterns exhibit low reflectance values in the visible bands (lower than 0.1), a significant increase in reflectance in the near-infrared band, and a decrease in the shortwave-infrared wavelengths. The ‘urban shadow’ and the ‘global dark’ both present very low reflectance values at all wavelengths. The ‘urban built-up’ and the ‘global substrate’ both show an increase in the reflectance as the wavelengths increase until the short-wave infrared. We can observe that both datasets show patterns for each target similar to those presented in the literature (Jensen, 2007). These patterns were manually searched for in both datasets, and in both cases, they represent most targets present in a satellite image.

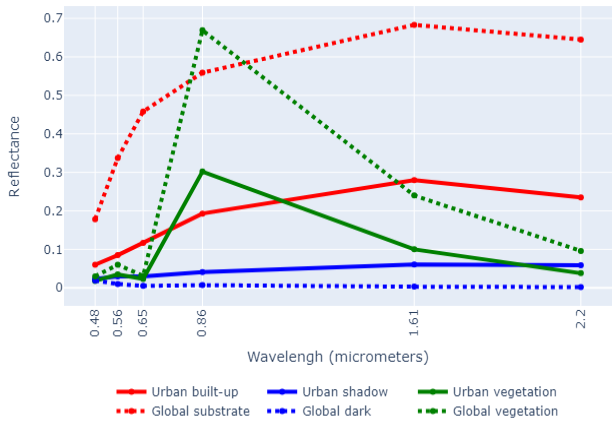

Figure 3. Endmembers’ reflectance spectral patterns.

The values of the ‘global dark’ endmember significantly lower in all bands compared to ‘urban shadow’, with the difference increasing with wavelength (Table 2). These differences can be attributed to atmospheric attenuation, which is strong at infrared wavelengths. The global coefficients were generated using subsets with water target in different regions of the Earth, including coastal areas where it is well-documented that models for the atmospheric correction do not work properly (Warren et al., 2019). For the other two endmembers, the global set of endmembers has values higher than the local set of endmembers (Table 2).

Endmembers	Landsat bands					
	B2	B3	B4	B5	B6	B7
Diference						
Buil-up	0.118	0.252	0.341	0.366	0.403	0.41
Shadow	-0.004	-0.02	-0.025	-0.034	-0.058	-0.057
Vegetation	0.012	0.025	0.008	0.367	0.14	0.058

Table 2. Different between global and local endmembers’ reflectance.

The Figure 4 shows the yearly variation in the abundance-images generated by LSMM for three different neighborhoods: ‘Restinga’, characterized by a large vegetated area, ‘Cidade Baixa’, with high density built-ups structure, and ‘Bom Jesus’, where many trees are spread out amidst the buildings. For each acquired date the average value for each endmember was calculated for each neighborhood. Despite the differences in magnitude, the temporal variations in each neighborhood show similarities in their interannual course. In this sense, the results support the notion that utilizing global endmembers in standardized mixture models can be advantageous, enhancing simplicity, consistency, inclusivity, and applicability, especially when the abundance-images will be use as input data for a classification or clustering procedure (Halbgewachs et al., 2022).

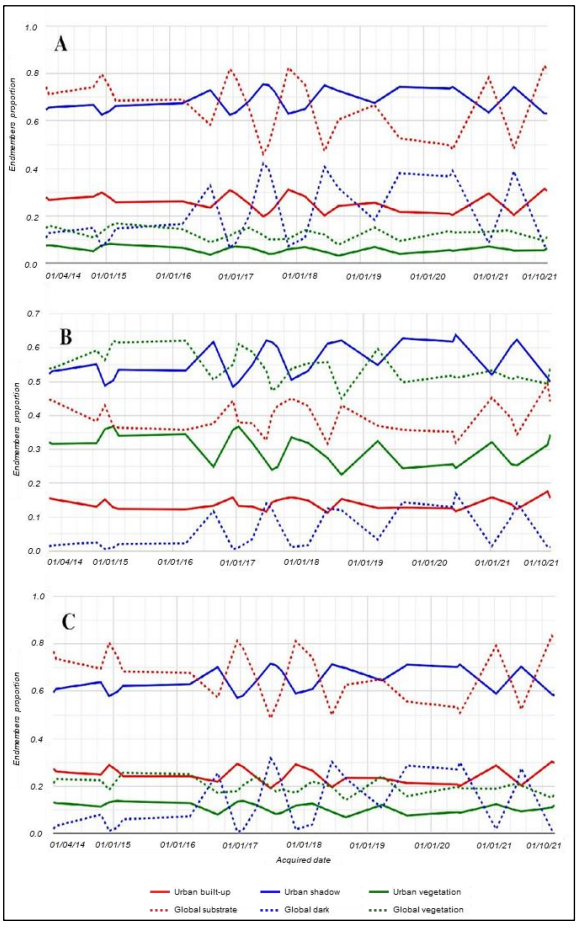

Figure 4. Estimated proportions for each endmember in all analysed dates for Cidade Baixa (A), Restinga (B) and Bom Jesus (C) neighbourhoods.

As we can observe in Figure 5, despite of endmember dataset (global or local), the areas with vegetation as well as areas with built-ups structures can be well identified in the color composite, allowing any clustering algorithm to identify and map these two different urban structures.

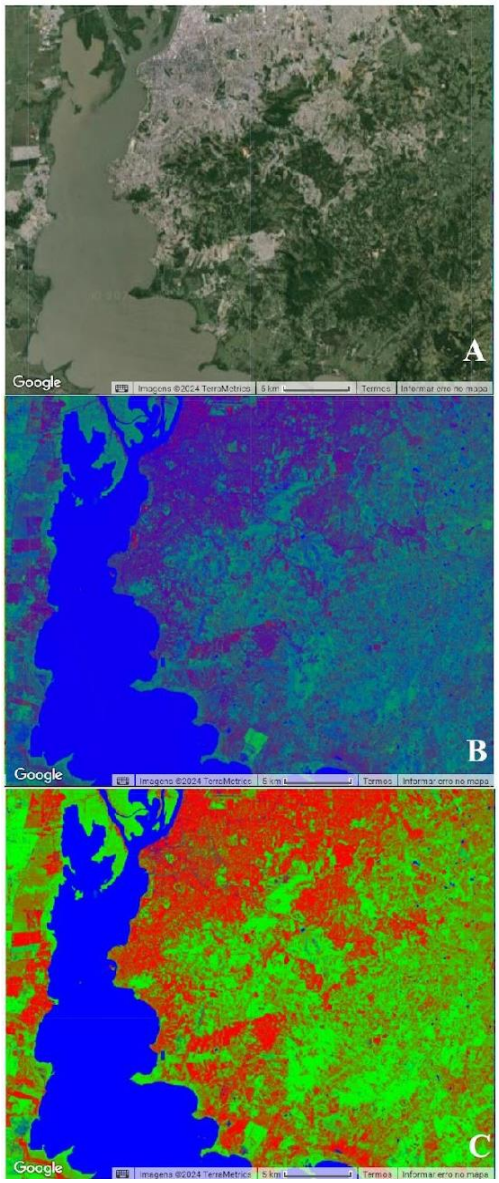

Figure 5. (A) Google base-map screenshot over Porto Alegre city. Abundance-images color composite (“Substrate / built-up”, “vegetation” and “dark / shadow” endmembers mapped in red, green and blue channels, respectively) (B) LSMM processed with (B) global endmembers and (C) local endmembers. Landsat 8, scene 221/081, 10/dec/2021.

The estimated proportion of each endmember using global patterns shows an overestimated ‘urban shadow’ for all analyzed images compared to proportions estimated using local patterns (Figure 4). Regarding the pixels used to define the endmember spectral pattern, the ‘urban shadow’ considered the same single pixel, over a building shadow target, collecting information from the 27 analyzed images. In contrast, for ‘global dark,’ the water pixels were considered to collect spectral information in 100 different subsets. The water, in fact, has near zero reflectance value in the NIR and SWIR wavelengths, whereas urban shadow is not a completely dark pixel because of the diffuse solar radiation it receives, resulting in some reflectance being detected in the infrared wavelengths. In the color composites (Figure 5), the influence of the ‘global dark’ endmember becomes evident. Built-up areas are characterized by a mixture of dark and substrate fractions, with substrate being more prominent in areas featuring brilliant roofs and bare soil.

In contrast, local endmembers are fine-tuned, optimizing outcomes tailored specifically for local LSMM. By accounting for the nuanced spectral characteristics inherent to the local environment, these endmembers contribute to a more precise understanding of the composition and distribution of targets within each studied area. In a detailed analysis, we can observe in Figure 6 the influence of the endmembers’ proportions based on the abundance-images color composite compared to the basemap (Figure 6A). Areas where both vegetation and built-up structures are predominant are well identified when the LSMM was performed using the local endmembers reflectance values (Figure 6C).

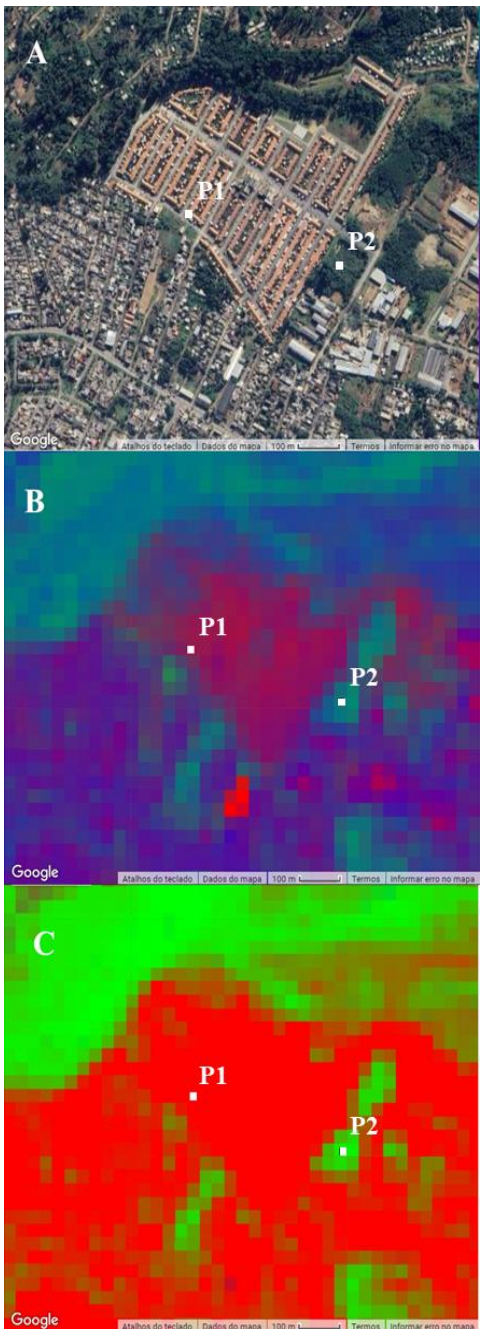

Figure 6. (A) Google base-map screenshot over Restinga neighborhood. Abundance-images color composite (“Substrate / built-up”, “vegetation” and “dark / shadow” endmembers mapped in red, green and blue channels, respectively) (B) LSMM processed with (B) global endmembers and (C) local endmembers. Landsat 8, scene 221/081, 10/dec/2021.

The Table 3 presents the proportions calculated for endmembers using global and local coefficients for a pixel with a predominance of built-up structures (Point 1, long: -51.138807 / lat: -30.143107) and for another pixel with a predominance of vegetation (Point 2, long: -51.136044, lat: -30.144987) (Figure 6B and 6C). We observe underestimation in pixels proportions obtained with the global coefficients. This discrepancy prevents the generation of maps of urban structures such as building or vegetation maps, based on proportion thresholds, as the estimated proportions do not correspond to the reality observed by the reference images (Figure 6A).

Endmembers	Point 1	Point 2
Global		
Substrate	0.615	0.019
Dark	0.288	0.497
Vegetation	0.095	0.482
Local		
Urban built-up	1	0.071
Urban shadow	0.0	0.0
Urban vegetation	0.0	0.929

Table 3. Global and local endmembers proportion

4. Conclusions

This study examined two distinct spectral patterns to assess urban structure estimation within Porto Alegre city, Brazil: one derived from global patterns acquired from 100 Landsat image subsets and the other from local patterns gathered across 27 analyzed images.

Results reveal that the utilization of global endmember patterns tends to overestimate the presence of urban shadow in all analyzed images compared to estimates derived from local patterns. Consequently, this overestimation impacts the relative proportions of other endmembers.

Despite the magnitude differences, the temporal variations exhibit interannual trends. In this context, the findings endorse the idea that using global endmembers in standardized mixture models can be beneficial, improving simplicity, consistency, inclusivity, and applicability. In contrast, local endmembers are fine-tuned to optimize outcomes specifically tailored for local LSMM. By considering the subtle spectral features specific to the local environment, these endmembers enhance a more accurate and detailed comprehension of the materials' composition and distribution of materials in each studied area.

Additionally, this investigation points to the importance of careful consideration of the features that must be represented in the resulting maps should guide the selection between global and local endmembers. Also, the processing level of the Landsat collections must be considered. The global coefficients were generated using Landsat Collection 1, which is currently deprecated, while the local patterns were generated using Landsat Collection 2.

Acknowledgements

This study was financed in part by the Coordenação de Aperfeiçoamento de Pessoal de Nível Superior - Brasil (CAPES) - Finance Code 001 – via scholarship to the second author PRINT UFRGS/POSGEA program.

References

Boeni, B., Silveira, D., 2019. Diagnóstico da arborização urbana em bairros do município de Porto Alegre, RS, Brasil. *Revista da Sociedade Brasileira de Arborização Urbana*, 6, 189.

Campana, N. A., Tucci, C. E. M., 2001. Predicting floods from urban development scenarios: Case study of the Dilúvio Basin, Porto Alegre, Brazil. *Urban Water*, *3*(1–2), 113–124. doi.org/10.1016/S1462-0758(01)00004-8

Ferreira, M. P., et al., 2020. Individual tree detection and species classification of Amazonian palms using UAV images and deep learning. *Forest Ecology and Management*, *475*, 118397. doi.org/10.1016/j.foreco.2020.118397

Gonçalves, A. P. S., Guadagnin, D. L., Padoin, N. P., 2020. Climate change and socio-economic vulnerability in the city of Porto Alegre. *Revista Brasileira de Gestão Urbana* 12(3), 1037–1054.

Gorelick, N., Hancher, M., Dixon, M., Ilyushchenko, S., Thau, D., Moore, R., 2017. Google Earth Engine: Planetary-scale geospatial analysis for everyone. *Remote Sensing of Environment*, *202*, 18–27. doi.org/10.1016/j.rse.2017.06.031

Guindon, B., Zhang, Y., Dillabaugh, C., 2004. Landsat urban mapping based on a combined spectral–spatial methodology. *Remote Sensing of Environment*, *92*(2), 218–232. doi.org/10.1016/j.rse.2004.06.015

Heinz, D. C., Chein-I Chang, 2001. Fully Constrained Least Squares Linear Spectral Mixture Analysis Method for Material Quantification in Hyperspectral Imagery. *IEEE Transactions on Geoscience and Remote Sensing* 39(3): 529–45. doi.org/10.1109/36.911111.

Halbgewachs, M., Wegmann, M., da Ponte, E., 2022. A Spectral Mixture Analysis and Landscape Metrics Based Framework for Monitoring Spatiotemporal Forest Cover Changes: A Case Study in Mato Grosso, Brazil. *Remote Sensing*, *14*(8). doi.org/10.3390/rs14081907

Instituto Brasileiro de Geografia e Estatística (IBGE), 2024. *Cidades@*. Available at: https://cidades.ibge.gov.br/brasil/rs/porto-alegre/panorama.

Jensen, J. R., 2007. *Remote sensing of the environment: an earth resource perspective*, 2nd ed. in Prentice Hall series in geographic information science. Upper Saddle River, NJ: Pearson Prentice Hall.

Lu, D., Weng, Q., 2004. Spectral Mixture Analysis of the Urban Landscape in Indianapolis with Landsat ETM+ Imagery. *Photogrammetric Engineering & Remote Sensing*, *70*(9), 1053–1062. doi.org/10.14358/PERS.70.9.1053

Lu, D., Weng, Q., 2004. Spectral Mixture Analysis of the Urban Landscape in Indianapolis with Landsat ETM+ Imagery. *Photogrammetric Engineering & Remote Sensing*, *70*(9), 1053–1062. doi.org/10.14358/PERS.70.9.1053

Nölke, N., 2021. Continuous Urban Tree Cover Mapping from Landsat Imagery in Bengaluru, India. *Forests*, *12*(2), Artigo 2. doi.org/10.3390/f12020220

Quintano, C., Fernández-Manso, A., Shimabukuro, Y. E., Pereira, G., 2012. Spectral unmixing. *International Journal of Remote Sensing*, 33 (17), 5307–5340. doi.org/10.1080/01431161.2012.661095.

Salbitano, F.; Borelli, S.; Conigliaro, M.; Yujuan, C., 2016. *Guidelines on Urban and Peri-Urban Forestry*. FAO: Rome, Italy.

Shimabukuro, Y. E., Smith, J. A., 1991. The least-squares mixing models to generate fraction images derived from remote sensing multispectral data. *IEEE Transactions on Geoscience and Remote Sensing*, *29*(1), 16–20. doi.org/10.1109/36.103288

Small, C., Milesi, C., 2013. Multi-scale standardized spectral mixture models. *Remote Sensing of Environment*, *136*, 442–454. doi.org/10.1016/j.rse.2013.05.024

Small, C., 2001. Estimation of urban vegetation abundance by spectral mixture analysis. *International Journal of Remote Sensing*, *22*(7), 1305–1334. doi.org/10.1080/01431160151144369

Stefanello, M., et al., 2023. Spatial–Temporal Analysis of a Summer Heat Wave Associated with Downslope Flows in Southern Brazil: Implications in the Atmospheric Boundary Layer. *Atmosphere*, *14*(1), doi.org/10.3390/atmos14010064

Tolan, J et al., 2023. *Very high resolution canopy height maps from RGB imagery using self-supervised vision transformer and convolutional decoder trained on Aerial Lidar*. arXiv.Org. doi.org/10.1016/j.rse.2023.113888

Twumasi, Y. A., et al., 2022. Fusion of Landsat 8 OLI and PlanetScope Images for Urban Forest Management in Baton Rouge, Louisiana. *Journal of Geographic Information System*, *14*(5), Artigo 5. doi.org/10.4236/jgis.2022.145024

Warren, M. A., *et al.*, 2019. Assessment of atmospheric correction algorithms for the Sentinel-2A MultiSpectral Imager over coastal and inland waters. *Remote Sensing of Environment*, vol. 225, pp. 267–289. doi.org/10.1016/j.rse.2019.03.018.

Zhang, H., Wang, X., Peng, D., 2022. Evaluation of Urban Vegetation Phenology Using 250 m MODIS Vegetation Indices. *Photogrammetric Engineering & Remote Sensing*, *88*(7), 461–467. doi.org/10.14358/PERS.21-00049R3

Zhang, X., Friedl, M. A., Schaaf, C. B., Strahler, A. H., Hodges, J. C. F., Gao, F., Reed, B. C., Huete, A., 2003. Monitoring vegetation phenology using MODIS. *Remote Sensing of Environment*, *84*(3), 471–475. doi.org/10.1016/S0034-4257(02)00135-9